Selective Stimulation of Penumbral Cones Reveals Perception in the Shadow of Retinal Blood Vessels

Manuel Spitschan[1], Geoffrey K. Aguirre[2]*, David H. Brainard[1]*

1 Department of Psychology, University of Pennsylvania, Philadelphia, Pennsylvania, United States of America, 2 Department of Neurology, University of Pennsylvania, Philadelphia, Pennsylvania, United States of America

* brainard@psych.upenn.edu (DB); aguirreg@mail.med.upenn.edu (GA)

Abstract

In 1819, Johann Purkinje described how a moving light source that displaces the shadow of the retinal blood vessels to adjacent cones can produce the entopic percept of a branching tree. Here, we describe a novel method for producing a similar percept. We used a device that mixes 56 narrowband primaries under computer control, in conjunction with the method of silent substitution, to present observers with a spectral modulation that selectively targeted penumbral cones in the shadow of the retinal blood vessels. Such a modulation elicits a clear Purkinje-tree percept. We show that the percept is specific to penumbral L and M cone stimulation and is not produced by selective penumbral S cone stimulation. The Purkinje-tree percept was strongest at 16 Hz and fell off at lower (8 Hz) and higher (32 Hz) temporal frequencies. Selective stimulation of open-field cones that are not in shadow, with penumbral cones silenced, also produced the percept, but it was not seen when penumbral and open-field cones were modulated together. This indicates the need for spatial contrast between penumbral and open-field cones to create the Purkinje-tree percept. Our observation provides a new means for studying the response of retinally stabilized images and demonstrates that penumbral cones can support spatial vision. Further, the result illustrates a way in which silent substitution techniques can fail to be silent. We show that inadvertent penumbral cone stimulation can accompany melanopsin-directed modulations that are designed only to silence open-field cones. This in turn can result in visual responses that might be mistaken as melanopsin-driven.

Introduction

A fine network of retinal vessels supplies the inner retina with blood [1–3], with decreasing vessel diameter towards the fovea. This network lies in front of the photoreceptive layer of the retina, thus casting shadows onto a set of cone photoreceptors. As the blood vessels are thin, most of the retinal cone mosaic is in the open light field, receiving unobstructed, incident light (Fig 1A). Cones positioned directly under the larger blood vessels lie in deep shadow and are

termed *umbral cones*. Between these two regions lies the *penumbra*, in which cones experience partial shadow [4]. As the shadow of the vasculature is stabilized on the retina it is not perceived under normal viewing conditions [5].

In 1819, the Bohemian physiologist Johann Evangelist Purkinje (Czech spelling *Jan Evangelista Purkyně*) found that moving a candle across the visual field allows an observer to view their own retinal blood vessels. This method displaces the shadow of the blood vessels on the retina, breaking stabilization and producing the entopic percept that we now refer to as the Purkinje tree ([6,7]; see Fig 2A). Visualization of the vasculature using kinetic techniques to move the shadow of the blood vessels has a rich history in vision science [8]. For example, Müller [9, 10] used it to deduce the location of the photoreceptive layer in the retina and more recently it has found a variety of clinical applications [11–34].

Here we demonstrate a novel method for visualizing the Purkinje tree, one that does not involve stimulus motion. The three classes of cones (L, M, and S) differ in their spectral sensitivity (Fig 1B). Light passing through hemoglobin is spectrally filtered. As a consequence, the cones that lie within the shadow of blood vessels have an altered spectral sensitivity relative to their open-field counterparts. The differential spectral sensitivity of open-field and penumbral cones allows these two populations to be selectively targeted using the method of silent substitution [35], with properly tailored spectral modulations. We report that selective stimulation of the penumbral L and M, but not S cones, elicits a clear percept of the retinal blood vessels.

Results

Using a digital spectral light modulator that produces a mixture of 56 narrowband primaries under computer control, we constructed sets of spatially-uniform spectral modulations that *a*) selectively stimulate penumbral cones (denoted as L^*, M^* and S^*) while silencing open-field cones (denoted as L, M and S), *b*) selectively stimulate open-field cones while silencing the penumbral cones, and *c*) stimulate open-field and penumbral variants conjointly. Each set includes one modulation that targets L and M cones, and a second modulation that targets S cones (Fig 1C; Appendix). Approximately 3–5% contrast was available within the gamut of our device for selective and differential stimulation of the penumbral and open-field L and M cones. That is, to produce more than this amount of contrast we would have to produce power less than zero at some wavelengths and/or power that exceeded that maximum available from our device at others. Approximately 20% contrast was available for the S cone variants. All modulations had zero predicted contrast on melanopsin. Modulations were presented around a high-photopic background (~2000 cd/m², Fig 1C) to saturate the rods. Table 1 provides the specific contrasts and background levels used for each modulation in each experiment. How we determined contrast is described in the Appendix (see Eq 2–4).

The output of the spectral light modulator was imaged onto a diffuser and viewed by observers through a custom eyepiece. The resulting stimulus configuration in all experiments was a spatially uniform annulus with a 27.5° outer diameter and with the central 5° obscured. Thin grid lines were etched into the diffuser to aid accommodation and fixation.

In informal observations, the three authors of this paper observed that when the penumbral L and M cone modulation was flickered at 8 or 16 Hz, a clear percept of the branching retinal blood vessels was produced within the stimulated portion of the visual field. This percept emerged at flicker onset, faded considerably over about a second, and could be restored if the flicker was halted and restarted. We do not have an explanation for the fading. Crucially, when viewing the stimulus with the right eye, the vessels appeared to converge to a point on the right side of the visual field, and vice versa when viewed with the left eye. This mirror symmetry is consistent with the structure of the image of the blood vessels on the retina.
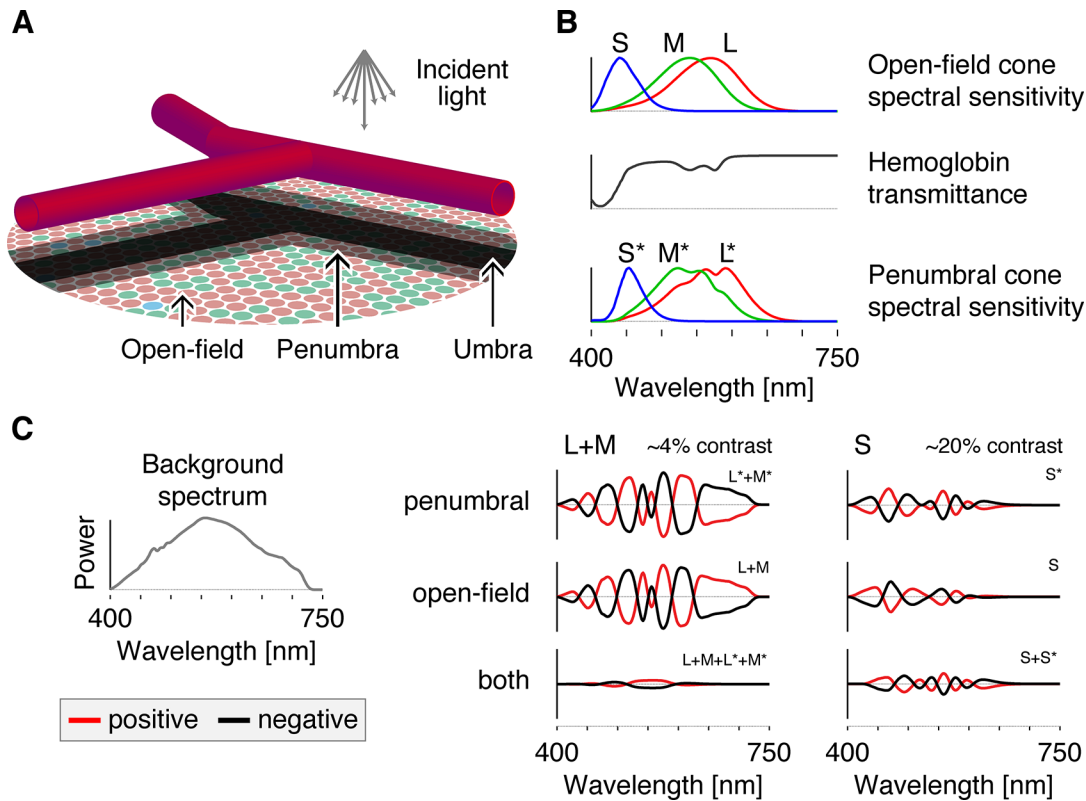
Fig 1. Spectral sensitivities and apparatus. A: Schematic diagram of the retina showing the shadows cast by the retinal blood vessels lying in front of the photoreceptive layer of the retina. B: The spectral sensitivities of the open-field cones (*upper panel*) are filtered by the hemoglobin transmittance spectrum (*middle panel*), resulting in wavelength-specific changes of the cone spectral sensitivities (*lower panel*). C: All modulations are carried out around a rod-saturating background whose spectrum is shown at the left. On the right are plotted the spectral modulations that target each of the indicated cone class(es), with the targeted class(es) indicated at the upper right of each individual plot. The amplitudes of these modulations are varied sinusoidally in time between the plotted positive (red) and negative (black) modulations and are then added to the background spectrum to produce the stimuli seen by the observer.

doi:10.1371/journal.pone.0124328.g001

We asked a naïve observer (female, 29 years old) to draw her percept in response to a pen-umbral-cone directed spectral modulation. She viewed a 16 Hz square-wave modulation of penumbral L and M cones monocularly with each eye in turn (the modulation viewed by this observer differed from those studied further below in that it did not silence melanopsin and consequently allowed a larger penumbral cone contrast; see Appendix and Table 1). The ob-server viewed the modulation and drew her entopic percept on a diagram that indicated both the obscured central 5° and the central grid lines superimposed on the uniform stimulus field (as shown in Fig 2B; the circle shown corresponds to the size of the 27.5° diameter field). The observer freely switched between the drawing and viewing the stimulus. The sketches produced by this observer are notable for their general resemblance to a Purkinje tree and may be com-pared with her actual vasculature as obtained from ocular fundus photographs of her two eyes (Fig 2C). The sketches capture the gross features of the larger blood vessels seen in the photos, with the larger vessels in the sketch emanating from the optic disk in both eyes and with smaller vessels shown branching from the larger ones. The implied location of the optic disks in the sketches (just inside the 13.75° eccentricity indicated by the circle) is consistent with their known anatomical positions in the retina [37]. A more detailed examination reveals that the correspondence between the sketches and photos is not exact; this may be a result of limits in the sketching ability of the observer. We also attribute to sketching imprecision the fact that

Table 1. Modulations and contrast values.

Direction	Task	Observer Age [yrs]	Observer ID	Mean luminance [cd/m²]	Chromaticity x	Chromaticity y	Pupil diameter [mm] Assumed	Pupil diameter [mm] Expected	Target contrast [%] (Expected absolute contrast splatter [%]) L	M	S	L*	M*	S*	Mel	Rods
L*+M*	Psychphysical rating task (n = 3) Main data	27	MS	1950	0.38	0.43	3	3.22	0.00 (0.12)	0.00 (0.10)	0.00 (0.32)	4.24	2.64	0.00 (0.67)	0.00 (0.39)	2.53 (2.52)
		44	GKA					3.06	0.00 (0.11)	0.00 (0.10)	0.00 (0.34)	4.18	2.58	0.00 (0.69)	0.00 (0.41)	2.66 (2.65)
		54	DHB					2.97	0.00 (0.11)	0.00 (0.11)	0.00 (0.37)	4.15	2.54	0.00 (0.79)	0.00 (0.44)	2.75 (2.75)
L+M		27	MS					3.22	4.06	2.87	0.00 (0.31)	0.00 (0.05)	0.00 (0.08)	0.00 (0.65)	0.00 (0.30)	-1.30 (1.28)
		44	GKA					3.06	3.89	2.95	0.00 (0.32)	0.00 (0.01)	0.00 (0.06)	0.00 (0.66)	0.00 (0.28)	-0.99 (0.98)
		54	DHB					2.97	3.71	3.07	0.00 (0.34)	0.00 (0.04)	0.00 (0.05)	0.00 (0.73)	0.00 (0.26)	-0.49 (0.48)
L+M+L*+M*		27	MS					3.22	5.00	5.00	0.00 (0.03)	4.44	4.57	0.00 (0.05)	0.00 (0.13)	1.89 (1.90)
		44	GKA					3.06	5.00	5.00	0.00 (0.03)	4.44	4.57	0.00 (0.05)	0.00 (0.14)	1.91 (1.91)
		54	DHB					2.97	5.00	5.00	0.00 (0.03)	4.45	4.57	0.00 (0.06)	0.00 (0.14)	1.91 (1.93)
S*		27	MS					3.22	0.00 (0.04)	0.00 (0.03)	0.00 (0.89)	0.00 (0.05)	0.00 (0.03)	20.00	0.00 (0.16)	-0.43 (0.43)
		44	GKA					3.06	0.00 (0.05)	0.00 (0.04)	0.00 (1.06)	0.00 (0.06)	0.00 (0.04)	20.00	0.00 (0.21)	-0.68 (0.68)
		54	DHB					2.97	0.00 (0.06)	0.00 (0.06)	0.00 (1.34)	0.00 (0.07)	0.00 (0.05)	20.00	0.00 (0.26)	-0.88 (0.88)
S		27	MS					3.22	0.00 (0.02)	0.00 (0.02)	20.00	0.00 (0.01)	0.00 (0.01)	0.00 (0.69)	0.00 (0.08)	0.47 (0.46)
		44	GKA					3.06	0.00 (0.04)	0.00 (0.04)	20.00	0.00 (0.04)	0.00 (0.03)	0.00 (0.91)	0.00 (0.17)	1.06 (1.06)
		54	DHB					2.97	0.00 (0.11)	0.00 (0.08)	19.81	0.00 (0.12)	0.00 (0.07)	0.00 (1.23)	0.00 (0.33)	2.18 (2.18)
S+S*		27	MS					3.22	0.00 (0.04)	0.00 (0.02)	20.00	0.00 (0.05)	0.00 (0.03)	20.00	0.00 (0.16)	-0.12 (0.12)
		44	GKA					3.06	0.00 (0.04)	0.00 (0.02)	20.00	0.00 (0.05)	0.00 (0.03)	20.00	0.00 (0.17)	-0.17 (0.17)
		54	DHB					2.97	0.00 (0.04)	0.00 (0.02)	20.00	0.00 (0.05)	0.00 (0.03)	20.00	0.00 (0.20)	-0.20 (0.21)
Melanopsin A	Psychphysical rating task (n = 3) Supplementarydata	27	MS					3.22	0.00 (0.20)	0.00 (0.20)	0.00 (0.66)	2.93 (2.94)	2.43 (2.42)	10.06 (10.10)	20.00	12.78 (12.76)
		44	GKA					3.06	0.00 (0.20)	0.00 (0.21)	0.00 (0.68)	2.85 (2.86)	2.35 (2.36)	9.03 (9.03)	20.00	12.75 (12.75)
		54	DHB					2.97	0.00 (0.20)	0.00 (0.25)	0.00 (0.79)	2.81 (2.83)	2.30 (2.27)	8.49 (8.59)	20.00	12.74 (12.68)
Melanopsin B		27	MS					3.22	0.00 (0.21)	0.00 (0.18)	0.00 (0.44)	0.00 (0.24)	0.00 (0.21)	0.00 (0.80)	20.00	11.86 (11.85)
		44	GKA					3.06	0.00 (0.21)	0.00 (0.19)	0.00 (0.45)	0.00 (0.23)	0.00 (0.22)	0.00 (0.79)	20.00	11.80 (11.80)
		54	DHB					2.97	0.00 (0.21)	0.00 (0.23)	0.00 (0.49)	0.00 (0.23)	0.00 (0.26)	0.00 (0.88)	20.00	11.77 (11.72)

(Continued)

Table 1. (*Continued*)

Direction	Task	Observer			Chromaticity		Pupil diameter [mm]		Target contrast [%] (Expected absolute contrast splatter [%])							
		Age [yrs]	ID	Mean luminance [cd/m²]	x	y	Assumed	Expected	L	M	S	L*	M*	S*	Mel	Rods
L*+M* +*Melanopsin*	Sketch	29	HW	2200	0.38	0.43	4.7	3.16	0.00 (0.60)	0.00 (0.97)	0.00 (0.78)	**7.73**	**5.58**	0.00 (2.67)	*41.35* (41.05)	*27.35* (28.05)

The table provides detailed information on the photoreceptor contrast expected for each of our stimulus modulations. Expected absolute contrast splatter was calculated according to the method outlined in the appendix. L*+M*, penumbral L and M cone modulation; L+M, open-field L and M cone modulation; L+M+L*+M*, modulation visible to both open-field and penumbral L and M cones; S*, penumbral S cone modulation; S, open-field S cone modulation; S +S*, modulation visible to both open-field and penumbral S cones. Individual observer ratings are shown to the right; Melanopsin A, melanopsin-directed modulation that did not silence penumbral cones; Melanopsin B, melanopsin-directed modulation with penumbral cones silenced; L*+M*+*Melanopsin*, penumbral L and M cone modulation ignoring melanopsin. Bold contrast values indicate the targeted photoreceptors. Italic contrast values indicate contrast not controlled for. Expected pupil diameter calculated using the unified formula for light-adapted pupil size from Watson and Yellott [36] assuming a 27.5° field and monocular illumination. This choice affects calculated retinal illuminance and thus the estimated fraction of cone pigment bleached used to construct cone spectral sensitivities. It would have been better to use a 3 mm pupil for observer HW, but the effect of the larger assumed pupil size is small (see Appendix).

doi:10.1371/journal.pone.0124328.t001

the sketches extend slightly beyond the indicated outer diameter of the stimulus field; the Purkinje tree percepts were always confined to the part of the visual field that was stimulated.

Consistent with our own percepts, the sketched Purkinje tree corresponds only to the larger retinal blood vessels, similar in spatial structure to those observed when a moving penlight is shown through the side of a closed eyelid. Finer vasculature extending in towards the fovea, which may be observed using other kinetic methods, was not visible using our method.

We conducted a rating experiment to measure three properties regarding the photoreceptor contributions to and temporal characteristics of the Purkinje-tree percept. First, we tested whether penumbral cone stimulation is necessary to produce the Purkinje-tree percept, or whether differential contrast between penumbral and open-field cones is both necessary and sufficient. Second, we considered that spatial contrast produced by the uniform spectral flicker is perfectly stabilized on the retinal surface, as the blood vessels move with the photoreceptors. Thus we predicted that the temporal dependence of the Purkinje-tree percept should have a bandpass shape similar to that found in measurements of temporal contrast sensitivity for retinally stabilized images [38,39]. Finally, we expected the Purkinje-tree percept to be more robust for penumbral L and M cone flicker as compared to penumbral S cone flicker, given the reduced spatial resolution of the S cone mosaic.

The three authors viewed 2-second trials consisting of sinusoidal flicker modulations, with 250 ms cosine windowing at the beginning and end of each trial. Tones demarcated the start and end of each trial (Fig 3A). The six spectral modulation directions depicted in Fig 1C were shown. Each combination of modulation direction and frequency was presented five times, with trial order randomized. The observer was blind to the particular modulation direction and frequency presented on each trial. On every trial, the observer was asked to rate his percept using a 0–3 scale (0 = little or no spatial structure visible in the flicker; 1 = some spatial structure visible, but structure did not resemble the Purkinje-tree percept; 2 = faint or partial Purkinje-tree percept visible; 3 = strong Purkinje-tree percept). A rating of 3 corresponded to the strongest percepts we had observed in our apparatus. These were very salient, as in the sketch
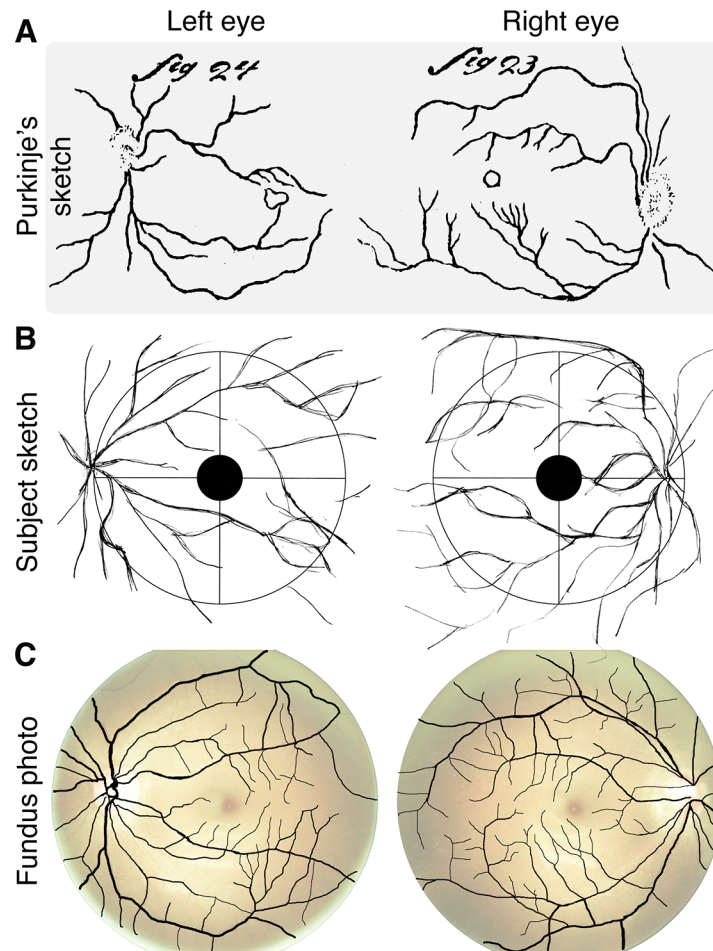
Fig 2. Purkinje-tree percepts. A: Sketch of entoptic visualization of retinal blood vessels from Purkinje ([7]; Figs 23 and 24). B: Sketch produced by a naïve observer in our study while viewing penumbral cone directed flicker at 16 Hz. C: Fundus photographs with overlaid extracted retinal blood vessels (see detailed methods in Appendix). The contrast and brightness of the fundus photographs were adjusted, and then made transparent for visualization purposes (see Fig 5 for raw fundus photographs). The fundus photos were obtained after the observer produced her sketches.

doi:10.1371/journal.pone.0124328.g002

shown in Fig 2. On 21 out of 231 trials, no modulation at all was shown (blank trials), to provide a control for false positives.

Both the selective penumbral L and M cone and the open-field L and M cone modulations elicited a clear Purkinje-tree percept at 16 Hz in all three observers (Fig 3B), with the strength of the percept falling off at lower and higher temporal frequencies. The control L and M cone modulation, which stimulated both open-field and penumbral L and M cones with similar contrast (much as would occur during natural viewing), did not elicit a Purkinje-tree percept. This confirms that time-varying differential contrast between open-field and penumbral cones is required to elicit a Purkinje-tree percept, and that this percept can be elicited by selective modulation of either penumbral or open-field cones.

The control L and M cone modulation did elicit faint percepts of spatial structure at temporal frequencies at and above 16 Hz, consistent with previous reports of flicker-induced visual field articulation at high frequencies [7,40–44]. All observers noted that this percept was
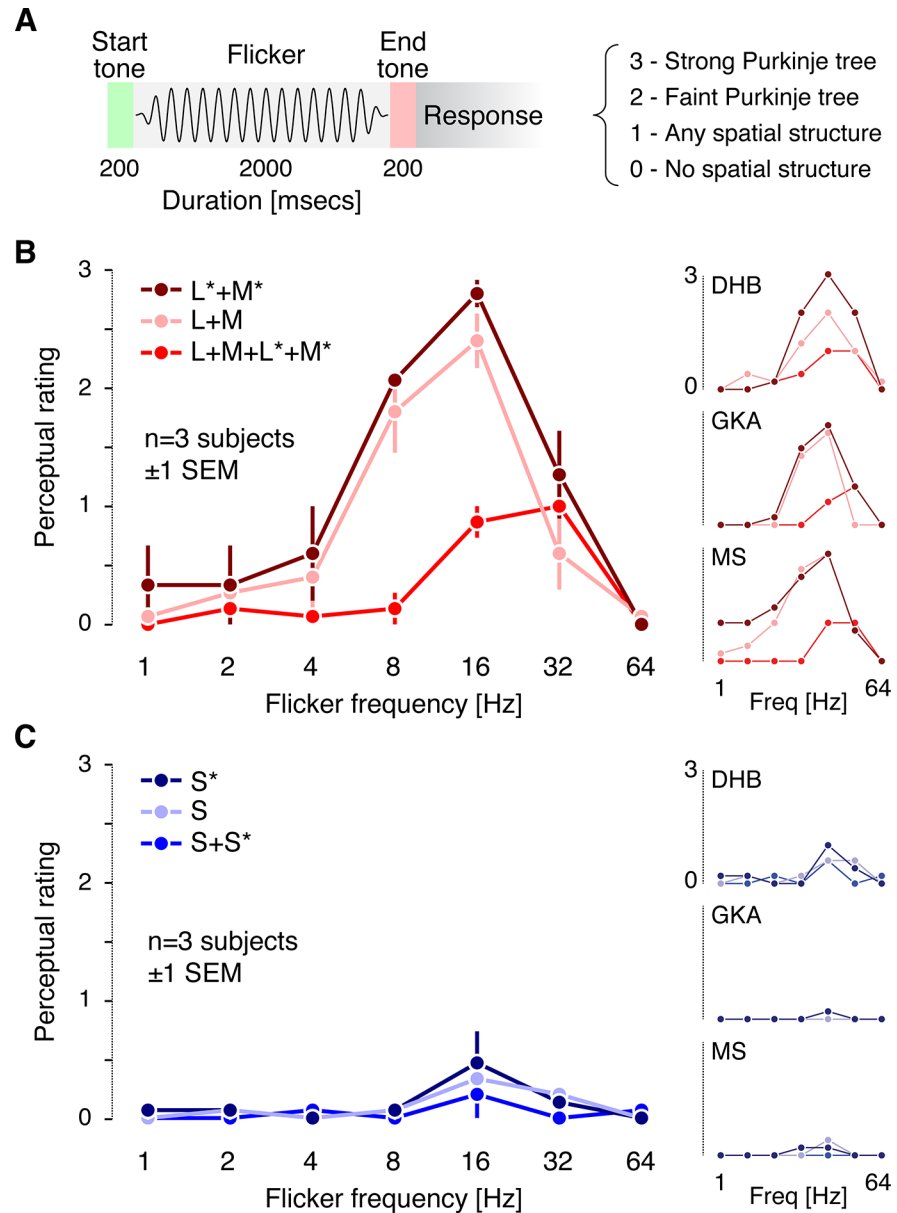
Fig 3. Psychophysical rating results. A: Time course of a single trial of the rating experiment and summary of the perceptual rating scale (see main text for more detailed description). B: Average ratings across the three observers for the L and M cone directed modulations. L*+M*, penumbral L and M cone modulation; L+M, open-field L and M cone modulation; L+M+L*+M*, modulation visible to both open-field and penumbral L and M cones. Individual observer ratings are shown to the right. C: Average ratings across the three observers for the S cone directed modulations. S*, penumbral S cone modulation; S, open-field S cone modulation; S+S*, modulation visible to both open-field and penumbral S cones. Individual observer ratings are shown to the right.

markedly different from that of the Purkinje tree. Blank trials did not lead to reported spatial structure (MS and GKA, all trials rated as 0; DHB 20 of 21 trials rated as 0, 1 trial rated as 1).

In contrast, selective stimulation of penumbral or open-field S cones did not produce a Purkinje-tree percept for any observer at any temporal frequency, although these modulations

could produce some non-specific spatial structure at 16 and 32 Hz ([Fig 3C]). Given the similarity of the temporal frequency dependence of the S cone ratings to those for L+M+L*+M*, it is possible that the S cone data are driven by residual contrast seen by L and M cones, as the precision of photoreceptor isolation is never perfect (see [Appendix]).

The trial-by-trial data for the rating experiment as well as the spectra of the modulations used are provided at [http://dx.doi.org/10.6084/m9.figshare.1327815]. This site also provides the data for the supplemental rating experiment (see below) and the spectra of the modulation presented to our naïve observer.

Discussion

A variety of methods to visualize one's retinal vasculature have been described since Purkinje's original observation. These have included: the use of stimulus motion under special conditions, most notably moving a small spot of light across the pupil [45]; very brief flashes illuminating the retina through the sclera causing a brief shift in the retinal position of the shadow of the vasculature [46]; the motion of corpuscles flowing through the vasculature [14,47–49]; long adaptation to dark, for example after lid closure during sleep [5,50–55]; intense illumination [56,57]; and pressure-induction [10,47,58]. These methods have been employed in a variety of studies that have determined the parameters needed to optimize entopic visualization [12,46,59–63].

Here we demonstrate a novel method for visualizing the Purkinje tree. Differential modulation of the L and M cones inside and outside the partial shadow of the retinal blood vessels produces a strong percept of one's retinal vasculature, when viewed at 16 Hz. We formalized this observation through a rating experiment, as well as through the sketches of a naïve observer. Our method is conceptually distinct from earlier kinetic techniques for blood vessel visualization: what changes over time in our method is the spectrum of a spatially uniform stimulus. This change in spectrum, rather than spatial motion of the shadow, stimulates penumbral cones differentially from the neighboring open-field cones and leads to the characteristic Purkinje-tree percept. Because our method does not involve spatial modulation of the image impinging on the photoreceptors, it provides a new tool for studying percepts arising from retinally stabilized images. For example, future work could use this technique to investigate in detail the fading of the Purkinje tree percept that we observe for continuously flickering stimuli.

Interestingly, the possibility of a spectral stimulus modulation that selectively drives the penumbral cones was suggested 50 years ago by Cornsweet [64], who wrote:

> "[I]t should be possible to provide a visual field in which the only thing that is changing is the stimulation of receptors behind blood vessels. This may be accomplished by showing the observer a field that is alternately lighted with 415 mμ [nm] and then with a mixture of two other wave lengths each of which is absorbed less strongly by blood, but so chosen that their mixture will match the 415 mμ [nm] light in regions not lying behind blood vessels." (p. 173)

The method we present here may be considered an implementation of Cornsweet's concept, albeit accomplished by a more complex spectral modulation than he envisioned. Our ability to construct an appropriate modulation is enabled by much more precise estimates of the cone fundamentals and their variation across the retina than were available in the 1960s [65–67].

We found that a temporal frequency of 16 Hz led to the strongest percept of the Purkinje tree, with weaker percepts at 8 and 32 Hz. These frequencies are somewhat higher than those

reported by Sharpe [59] for visualization of the Purkinje tree using a kinetic method, and higher than the peak of the temporal contrast sensitivity functions for stabilized retinal images [38,39]. In the former case differences might be expected because our stimulus does not involve any retinal motion, and in the latter because the temporal contrast sensitivity functions will depend on retinal location and the spatial structure of the stimulus as well as possibly the quality of image stabilization. Coppola and Purves [46] concluded from their kinetic-based studies of the Purkinje-tree percept that optimal stimulation frequencies were greater than 10 Hz. Our results are commensurate with this conclusion, although the data on which it is based were obtained for more central visualization of small capillaries rather than for the shadows of larger peripheral vasculature revealed by our method.

In a series of careful anatomical studies, Adams and Horton [4, 68, 69] demonstrated that the photoreceptors under retinal blood vessels have a corresponding area of decreased cortical representation in the squirrel monkey visual cortex, akin to a local form of amblyopia. The altered cortical representation was present even for smaller vessels that produce only penumbral shadow, and the width of the reduced cortical representation was wider than the shadows themselves. We find that the selective stimulation of the penumbral cones results in a visible percept. Thus, the reduced cortical representation identified by Adams and Horton [4, 68, 69] is not so extreme as to render penumbral cones inoperative or to eliminate the possibility of spatial vision mediated by these cones.

Our result has practical implications for the study of visual processes. For example, there is current interest the melanopsin-containing intrinsically photosensitive retinal ganglion cells [70–92]. Studies of melanopsin function in the mouse are facilitated by the use of transgenic photoreceptor knock-out models [75,76,93]. These techniques are obviously not available for studies of human observers. Because of the overlap in spectral sensitivity of the cones and melanopsin, functional isolation of melanopsin in humans has been approached using the method of silent substitution [84,90,94–96]. As typically implemented, modulations that target melanopsin and silence the open-field cones will produce residual stimulation on the penumbral cones. In their recent paper, Horiguchi et al. [82] calculated that such residual stimulation exceeds the cone detection threshold and noted the possibility that the effects of such stimulation might account for some of their psychophysical results, particularly the surprising observation that in the periphery observers could detect nominally cone-silent modulations at 40 Hz. We calculated that the nominally melanopsin-isolating direction in the study of Horiguchi et al. [82] produced 1–2% contrast on penumbral cones. In our recent study of photoreceptor contributions to the pupillary light reflex [94], the primary melanopsin-directed modulation employed also produced residual stimulation of penumbral cones of similar magnitude. Our demonstration here that a small degree of selective penumbral cone contrast produces a clearly visible percept should prompt caution regarding the interpretation of results obtained using silent substitution, particularly under conditions where penumbral-cones might plausibly mediate the measured response of interest. Similar warnings have been issues previously regarding variation of cone spectral sensitivity across the retina as a function of changes in pre-retinal filtering [97,98] and with respect to individual variation in cone spectral sensitivities [82].

It is possible to produce spectral modulations that target melanopsin with about 20% contrast while nominally silencing both open-field and penumbral cones. Indeed, in a supplemental rating experiment, we found that controlling for the stimulation of penumbral cones reduces or removes the Purkinje-tree percept, which is otherwise visible for a melanopsin-directed modulation (see Appendix). While even a small degree of penumbral cone contrast produces a prominent perceptual effect at 16 Hz, we have found that failure to control for this inadvertent stimulation has minimal effect upon measured pupil responses at low temporal

frequencies [94]. Consequently, the degree of attention needed to the effect of cones lurking in the vascular shadows will vary, depending upon the response being measured.

Appendix: Detailed Methods and Supplemental Experiment

Subjects

The three authors of the study served as observers. All three are male, have corrected visual acuity of 20/20 or better and normal color vision as judged by Ishihara color plate screening [99]. At the time of data collection their ages were: MS 27, GKA 44, DHB 54. The research was conducted in accord with the principles of the Declaration of Helsinki and approved by the University of Pennsylvania Institutional Review Board. Informed written consent was obtained from all observers.

Apparatus

The apparatus is discussed in detail in Spitschan et al. [94]. We used the method of silent substitution [35,100] in combination with a spectral light modulator (OneLight VISX Spectra Digital Light Engine), which produces light with arbitrary spectral power distributions. The theory of operation of the modulator is as follows: Light from a Xenon arc lamp passes through a slit, is collimated, then passed through a diffraction grating. This separates the light into individual narrowband wavelength components. Each component is then imaged onto a column of a digital light processing (DLP) chip (1,024 columns x 768 rows). Each row on this chip can be turned on or off independently in each column, thus allowing for the selective control over the exitant power in each wavelength band. Rather than addressing the 1,024 columns separately, we treated groups of 16 columns as single primaries, resulting in 56 independent nearly monochromatic primaries (after turning off 80 columns at the short wavelength end of the spectrum, and 48 columns at the long wavelength end of the spectrum, where there was too little light power for us to measure accurately). This grouping of columns provided us with 768 x 16 = 12288 discrete power levels for each primary; the spectral width of the primaries (~16 nm FWHM) was dominated by the spectral bandwidth of the optical system rather than the width of a column on the DLP chip, and there was little spectral shift with output power for our 56 primaries. The DLP chip can modulate rapidly. In the experiments reported here we use it in a mode where we control the emitted spectra at 256 Hz.

The monochromatic primaries leaving the DLP chip were mixed and transmitted through a fiber optic cable (FTIIG16860-40, total length 40 feet; Fiberoptics Technology, Inc.), passed through IR and UV blocking filters, and illuminated a diffuser within a custom-made eye piece. Observers viewed an image of the diffuser through a 25 mm focal length lens, resulting in a 27.5° spatially uniform field with the central 5° blocked by an opaque circular occluder mounted on the diffuser. The diffuser also contained then etched grid lines to facilitate accommodation and fixation by the observer.

The power at each wavelength for each of the 56 primaries was measured through the eyepiece using a spectraradiometer (PR-670 SpectraScan, Photo Research). Each primary was measured at 16 power levels, which allowed us to characterize the nonlinearities between the device primary settings and the exitant light power. We verified that the light emitted from the spectral modulator with all mirrors turned on contained no appreciable power in the UV (200–380 nm) or NIR (780–1020 nm) wavelength ranges using fiber spectrometers (two customized Ocean Optics USB2000+ spectrometers with ILX-511B detector; wavelength ranges 180 nm–875 nm and 340–1025 nm, respectively; 3 m custom Ocean Optics fiber-optic cable). We calculated that the light power in the visible range of the spectrum (380–780 nm) was

within light safety standards [101] and provide example code for light safety calculations in the Silent Substitution Toolbox (see below, http://silentsubstitutiontoolbox.org).

Construction of Spectral Modulations

Because we have available 56 primaries, there are many physically distinct spectral modulations that can be produced by our device and that satisfy a set of specified photoreceptor-silencing constraints. To choose a specific modulation, we have developed general methods that allow us to trade off between several criteria. First, we wanted spectral modulation directions that maximized contrast on targeted photoreceptor classes, within the gamut limits of our stimulation device [102,103]. Second, to the extent possible, we wanted the modulation to vary smoothly with respect to wavelength. This second requirement was imposed based on the intuition that small deviations between the desired modulation and that actually produced by the device will have a smaller effect on nominally-silenced photoreceptors for spectrally smooth modulations than will modulations that vary rapidly as a function of wavelength. Third, we wanted the contrasts produced by the modulations, particularly their ability to silence photoreceptor classes, to be robust with respect to uncertainty in our estimates of the spectral sensitivity of the nominally silenced photoreceptors. To choose modulations that are consistent with these criteria, we implemented a constrained numerical optimization procedure. We have made our software available under an open-source license (Silent Substitution Toolbox; http://silentsubstitutiontoolbox.org). This provides a MATLAB implementation, as well as methods for obtaining estimates of photoreceptor spectral sensitivities (in conjunction with software and data provided in the open-source Psychophysics Toolbox; Brainard [[104], http://psychtoolbox.org]) and methods for computing what we refer to as contrast splatter maps (see Precision of Photoreceptor Isolation section below). Our software takes advantage of the sequential quadratic programming (SQP) algorithm provided in the function *fmincon* in MATLAB's Optimization Toolbox.

To find desired modulations in the 56-dimensional device primary space, we divide the photoreceptor classes under consideration into three sets. We call these the targeted set, the silenced set, and the ignored set. We search over device primary settings to maximize the contrasts seen by the photoreceptor classes in the targeted set, subject to the constraints i) that the contrasts seen by the photoreceptors in the silenced set are zero and ii) that the device primary settings are within gamut. More specifically, we minimize the quantity

$$f = \sum_m (C_m - 1)^2 \tag{1}$$

where m indexes the photoreceptor classes in the targeted set and c_m is the contrast seen by the mth class in the set. The quantity f is minimized when the contrasts in the targeted set are as close to 1 as can be obtained subject to the constraints described below. We generally seek spectral modulation directions for which equal positive and negative contrasts around the specified background may be obtained within gamut around the specified background, so that 1 is the maximum obtainable contrast. As a practical manner, our code enforces the device gamut constraints for both the positive and negative modulations during the numerical optimization.

The optimization also enforces a smoothness constraint on the modulations: the maximum absolute difference in spectral power between adjacent sample wavelengths was required to be below a specified criterion. The exact choice of criterion depends on the size of the wavelength sampling step and the intensity of the spectral background, and it can be adjusted to tradeoff between maximal obtainable contrasts for the targeted set and the spectral smoothness of the obtained modulation spectra. This is a choice we make manually for each application of our

procedures. For the modulations used in this paper, the wavelength sampling was 380 nm to 780 nm in 2 nm steps, the criterion was $10^{-1.5}$ watts/[m²·sr] relative to a background spectrum with total radiance of about 11.7 watts/[m²·sr].

To compute the contrasts for each photoreceptor class, we use device calibration information to compute the predicted spectrum from the device settings. This, together with specification of a background spectrum, allows the computation of contrasts. Typically, we chose the background spectrum $B(\lambda)$ to be that produced by the mixture of all primaries at half their maximum power. Suppose there are n classes of photoreceptor under consideration, whose spectral sensitivities $S_n(\lambda)$ are known. We compute the receptor responses of each class to the background b_n as

$$b_n = \sum_n S_n(\lambda) B(\lambda) \delta \lambda \tag{2}$$

Similarly, for any other spectrum $M(\lambda)$, we compute the receptor responses m_n as

$$m_n = \sum_n S_n(\lambda) M(\lambda) \delta \lambda \tag{3}$$

This yields the contrast seen by each photoreceptor class between the between $M(\lambda)$ and $B(\lambda)$ as

$$c_n = \frac{m_n - b_n}{b_n} \tag{4}$$

To make the silent-substitution properties of the modulations robust to uncertainty about the spectral sensitivities of the specified photoreceptor classes, we add to the silenced set of photoreceptors not only the nominal versions of the silenced photoreceptor classes but also variants of the nominal versions that represent individual variation. Effectively, the set of silenced photoreceptors provides a basis that spans a larger space of silenced photoreceptor sensitivities. For example, if we are silencing the open-field cones, we have the option of adding to the silenced set variants of the open-field cones computed with higher and lower lens densities than the nominal versions. Whether this is desirable to do again involves a tradeoff that we make manually. The more photoreceptor variants we add to the silenced set, the more robust the modulations but the lower the maximum contrast achievable for the targeted set. We make this tradeoff through examination of the maximum achievable contrasts and of "contrast splatter maps", which are described below. For the modulations used in this paper, we did not in the event add additional photoreceptor classes to the silenced set, because we wanted to produce as much differential contrast as possible between penumbral and open-field cones. In other work [94], we have found it beneficial to increase robustness in the manner described here.

Sometimes it is desirable not to maximize the contrast for the photoreceptor classes in the maximized set, but rather to produce modulations that have specified target contrasts for each class in this set. For example, for the supplemental experiment reported in this paper we produced modulations that had the same 20% contrast on melanopsin with and without stimulating the penumbral cones. This is achieved in our software by replacing the objective function that seeks to maximize the contrast of the classes in the maximized set with a modified objective function that seeks to bring these contrasts as close as possible to a set of specified target contrasts t_m. Specifically, in this case the optimization routine seeks to minimize the sum of squared deviations

$$f = \sum_m \left(C_m - t_m\right)^2 \tag{5}$$

between the predicted contrasts c_m and the targeted contrasts t_m for the members of the targeted set. In practice, we generally begin by finding the maximum available contrast on classes in the maximized set and then choosing targeted contrasts based on this information.

The contrasts of the photoreceptor classes in the ignored set are disregarded in the optimization. For example, when we compute modulations for use in studies at high photopic light levels, we often place the rod spectral sensitivities in the ignored set. The reader may note that this could also be accomplished simply by not specifying the ignored classes in the set of photoreceptor spectral sensitivities under consideration. We find the code more transparent if we allow for explicit specification of what classes are ignored, as this allows use of a single set of receptor sensitivities across multiple calls to the optimization routine. The calculation of a given desired spectral modulation takes <400 ms in MATLAB on a current (2014) desktop computer.

Estimates of Photoreceptor Sensitivities

Spectral sensitivities of the open-field L, M and S cones at the cornea were calculated using the CIE 2006 parametric model and incorporate pre-retinal filtering due to lens, ocular media and macular pigment using the age, pupil size and field size dependences of that model [66]. Pre-retinal filtering for all spectral sensitivities was computed using the actual age of each observer and the appropriate field size (27.5°). Although the CIE standard specifies a very small but non-zero amount of macular pigment density outside the central 5°, the contribution of macular pigment filtering to the cone fundamentals for our stimulus configuration is minimal. We adjusted the peak optical density of the cone photopigments depending on the expected proportion of bleached photopigment [105,106] for the retinal illuminance of our rod-saturating background stimulus. For the psychophysical rating task (observers MS, GKA, DHB), we assumed a pupil diameter of 3 mm in computing retinal illuminance, corresponding to the natural light-adapted pupil. For the sketch drawing, we assumed a pupil diameter of 4.7 mm, which is slightly higher than the expected light-adapted pupil size for that light level (Table 1; [36]).

We obtained spectral sensitivities for the penumbral cones by assuming that hemoglobin acts as a pre-retinal filter. We calculated the hemoglobin transmittance spectrum as follows, following the calculations of Horiguchi et al. [82]. We obtained estimates of the molar extinction coefficients e of oxyhemoglobin (HbO_2) and deoxyhemoglobin (Hb) expressed in [cm^{-1}/(moles/liter)] [107]. To convert this to the absorptivity, we multiplied by the constant 2.303 and the molar concentration of oxyhemoglobin and deoxyhemoglobin, given by $\frac{150 \text{ gHb/liter}}{64,500 \text{ gHb/mole}}$ [107], giving the *absorptivity* coefficients A_{HbO_2} and A_{Hb}, expressed per μm. We assumed an optical path length through the vessels of 11.5 um for penumbral cones, thus obtaining *absorptance* coefficients $a_{HbO_2} = 11.5 A_{HbO_2}$ and $a_{Hb} = 11.5 A_{Hb}$. This diameter corresponds to the size of venules or smaller arterioles. We combined these to get overall absorptance as follows. We assumed that oxyhemoglobin makes up 95% of the hemoglobin in arteries and 75% of the hemoglobin in veins at room air oxygenation following the oxygen-hemoglobin dissociation curve of adult hemoglobin [108], and took the average between these two to set the fraction of oxygenated hemoglobin at 85%. The overall absorptance was computed as $0.85 a_{HbO_2} + 0.15 a_{Hb}$ and the transmittance was then obtained as $10^{-(0.85 a_{HbO_2} + 0.15 a_{Hb})}$.

We constructed the spectral sensitivity of melanopsin along the lines of a recently proposed standard for 'melanopic' sensitivity [109] by shifting the Govardovskii nomogram [110] to have its peak spectral sensitivity λ_{max} at 480 nm, consistent with previous reports of the peak spectral sensitivity of melanopsin [111–113]. We assumed an optical density of 0.015 [114]. For melanopsin, pre-retinal filtering was incorporated as for the cones, except for filtering due

to macular pigment, which was omitted altogether because the melanopsin-containing retinal ganglion cells lie in front of the macular pigment layer.

Precision of Photoreceptor Isolation

To estimate the uncertainty of the method of silent substitution given our apparatus, we calculated *contrast splatter*, which is the expected amount of contrast on nominally silenced photoreceptor classes for a given modulation around a given background. This was done by calculating contrast across variants of photoreceptor sensitivity obtained by shifts in the assumed wavelength of photopigment peak absorbance (λ_{max}) and varying observer lens density using age as the parameter describing lens density according to the CIE formula [66]. Shifts of photopigment absorbance were accomplished by using the Stockman-Sharpe nomogram, which provides a formula that yields the full photopigment spectral absorbance spectrum given a specified wavelength of peak absorbance λ_{max} [65]. A calculation was performed for each photoreceptor class in which we varied λ_{max} by ±10 nm and let the age parameter vary between 20 and 60 years. In estimating the spectral sensitivities of the photoreceptor variants, we did not recalculate the estimate of fraction of cone photopigment bleached for each variant. Fig 4 shows the results of the splatter calculation. In panel A, for example, the top two pseudocolor plots show the computed contrast splatter map for each variant of the open-field L cones and penumbral L cones, for a 27 year old observer (MS), for the L and M penumbral cone modulation. Computed contrast matches the nominal values (0% for open-field L cones; 4.2% for penumbral L cones) for the targeted λ_{max} (558.9 nm) and observer age (27), and deviates from the nominal values for other L cone variants.

Using estimates of the variability of λ_{max} and lens density in the population of normal color observers, we then constructed 95% and 99% confidence ellipses for these parameters, based on the assumption that variability is normally and independently distributed for both λ_{max} and lens density. We also calculated the expected absolute contrast splatter, which is the expected absolute value of the deviation between obtained and targeted contrast for the silenced photoreceptors, based on the same assumption. We assumed standard deviations of 1.5, 0.9 and 0.8 nm for L, M and S cone λ_{max} variation around the nominal values [115]. We extracted the standard deviation of the veridical measurement residuals vs. chronological age from a two-component lens density model [116] and found that the standard deviation of the predicted age parameter of lens density due to individual variation is 7 years. For nominally silent photoreceptor classes, the expected absolute contrast splatter does not exceed 1.23% for any observer, modulation direction, and photopigment absorbance variant (Table 1). Additional contrast splatter may arise because of limitations of stimulus control. We periodically assess this via direct measurement of the spectra produced by our stimulus device, and find that it is of the same order as the contrast splatter we expect from uncertainty in photoreceptor sensitivities.

We considered the possibility that the modulation that nominally drove open-field and penumbral cones together (L+M+L*+M*) in practice elicited substantial differential contrast between the open-field and penumbral cones. To test this, we constructed contrast splatter maps for this modulation (Fig 4, panel C) for the 27 year old observer (MS). For each photoreceptor variant we then plotted the contrast seen by the penumbral L and M cones against the contrast seen by their open-field counterparts (Fig 4, panel D). We find that the contrasts seen by the open-field and penumbral cones are similar to each other across all of the photoreceptor variants, indicating that this key property of the modulation is highly robust with respect to variation in photoreceptor spectral sensitivity. The differential contrast of penumbral cones relative to open-field cones for our penumbral L and M modulation is similarly robust (Fig 4, panel B).
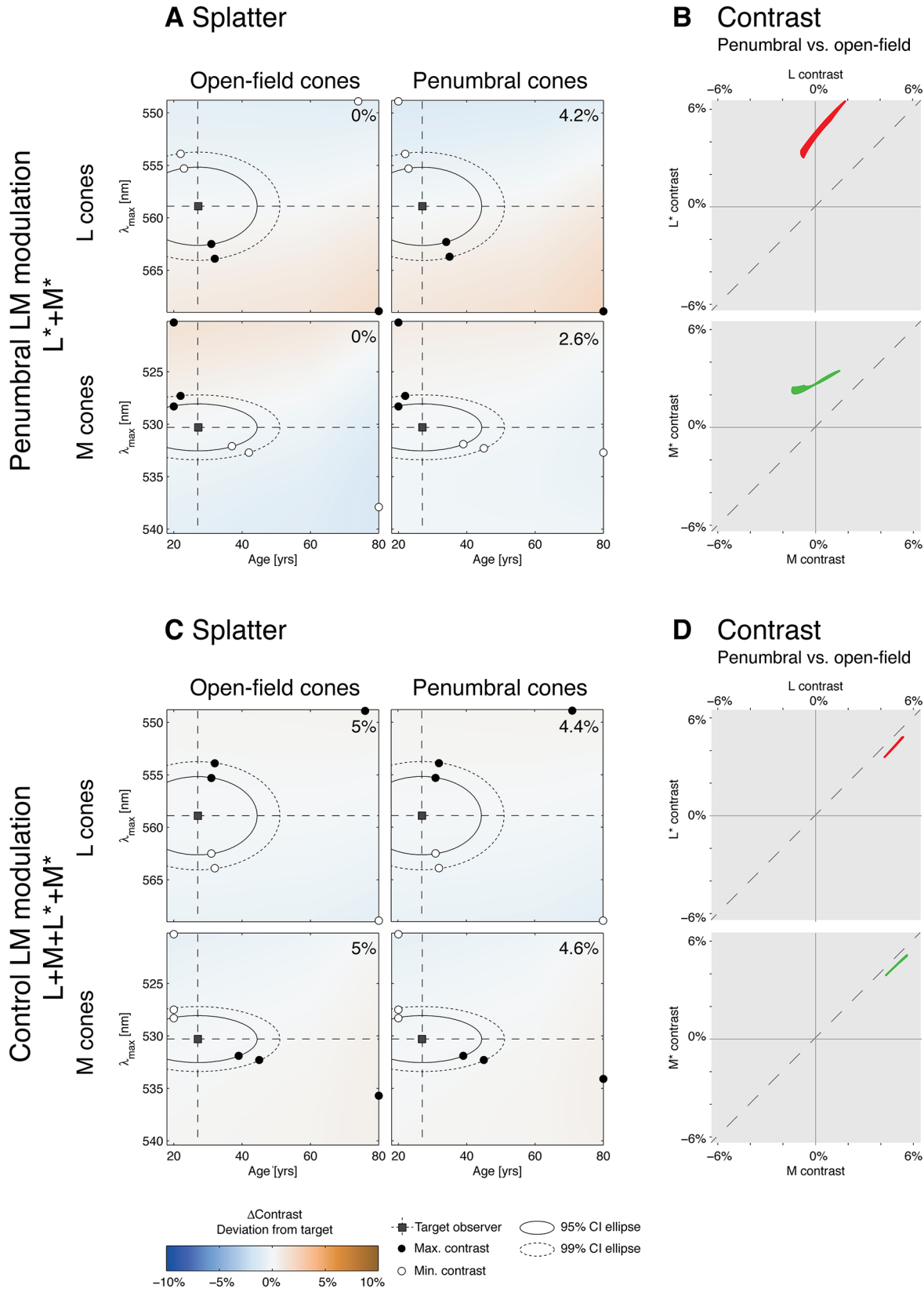
Fig 4. Contrast splatter. A: Contrast splatter calculations for the penumbral L and M cone (L*+M*) modulation (27 year old observer). Separate splatter maps for open-field and penumbral L and M cones are provided. Each point in a splatter map indicates in pseudocolor the contrast that will be seen by a variant of the nominal cone spectral sensitivity, as indicated by its position on the age and λ_{max} axes. The color scale is provided at the bottom of the figure, with negative contrast splatter indicating contrast splatter that is 180° out-of-phase with the nominal stimulus modulation. The open square indicates age and λ_{max} of the nominal cone spectral sensitivity, while the solid and dashed ellipses indicate the 95% and 99% confidence ellipses for variation around the nominal sensitivity. Open and closed circles on each ellipse show the variant with the minimum and maximum contrast splatter on the ellipse. Open and closed circles on the edges of the map represent the variant with minimum and maximum contrast splatter over the whole range of variants computed. The nominal contrast of the modulation for each cone type is provided in the upper right of each map. B: Comparison of contrast seen by the penumbral vs. open-field L cones across the entire range of photoreceptor variants studied in panel A (top plot) and similarly for the M cones (bottom plot). C: Contrast splatter maps for the modulation that stimulated both penumbral and open-field L and M cones together (27 year old observer). Same format as panel A. D: Same type of comparison as shown in panel B, obtained from the splatter maps shown in panel C.

doi:10.1371/journal.pone.0124328.g004

Fundus Photos

The fundus photographs for our naïve observer ([Fig 2C] and [Fig 5]) were obtained using a NIDEK Microperimetry device (MP1). For visualization purposes, the retinal vasculature ([Fig 2C] overlay) was manually extracted from the photograph with Adobe Photoshop using a combination of image feature selection techniques, and the contrast and color balance of the photos was adjusted for visualization purposes. A raw version of the fundus photos is provided in [Fig 5].

Supplemental Experiment

In a supplemental experiment, we tested whether a melanopsin-directed modulation designed to silence open-field but not penumbral cones can elicit percepts of the Purkinje tree, and whether this is due to contrast seen by penumbral cones ([Fig 6]). Observers viewed two mela-nopsin-directed modulations. The *Melanopsin A* modulation was constructed using a target contrast for melanopsin of 20% with open-field L, M and S cones silenced. Stimulus contrast was not constrained for penumbral cones, however, and this resulted in a *Melanopsin A* modulation that produced ~2–3% contrast on penumbral L and M cones and ~10% contrast on penumbral S cones ([Table 1]). The *Melanopsin B* modulation was constructed again using a target contrast of 20% for melanopsin, but with both open-field and penumbral cones silenced. As control modulations, we added the L and M penumbral cone directed modulation and a
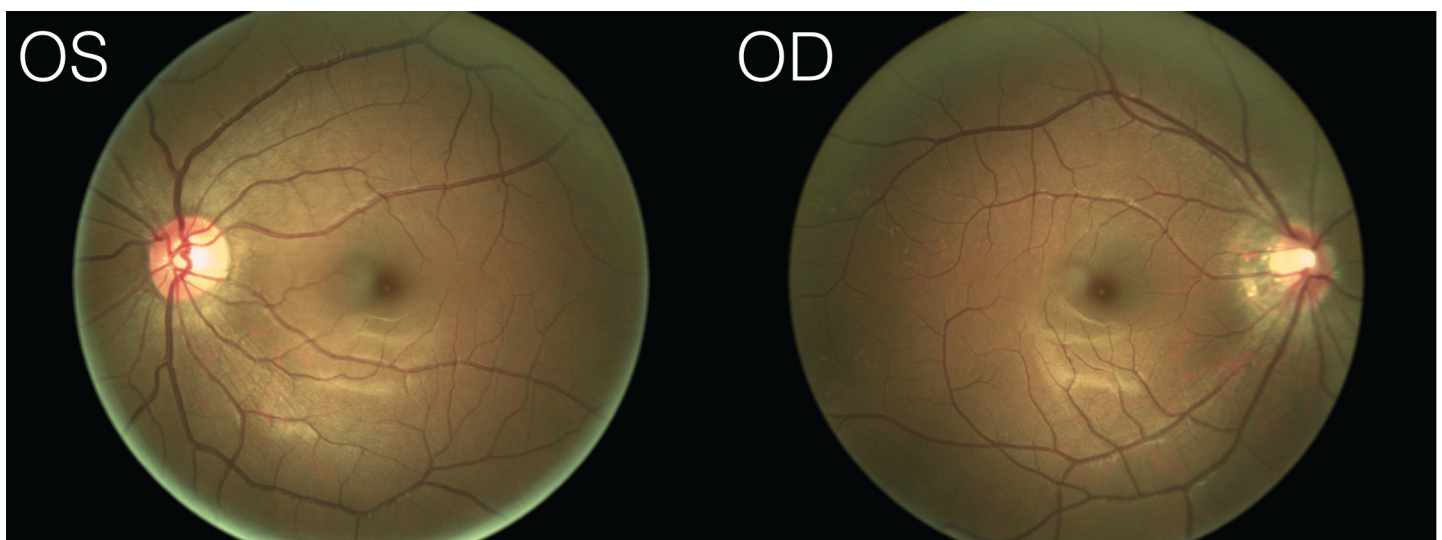
Fig 5. Raw fundus photographs. Unedited fundus photographs (OS = left eye, OD = right eye) obtained for our naïve observer.

doi:10.1371/journal.pone.0124328.g005
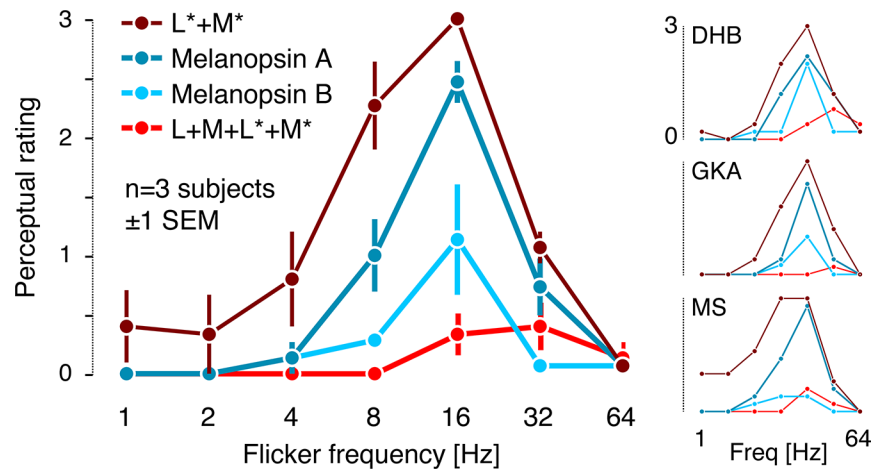
Fig 6. Rating data from the supplemental experiment. Average ratings across the three observers. L* +M*, penumbral L and M cone modulation; Melanopsin A, melanopsin-directed modulation that did not silence penumbral cones; Melanopsin B, melanopsin-directed modulation with penumbral cones silenced; L +M+L*+M*, modulation visible to both open-field and penumbral L and M cones. Individual observer ratings are shown to the right.

doi:10.1371/journal.pone.0124328.g006

modulation stimulating both sets of L and M cones together while silencing the other photo-pigments. These latter two modulations were as in our main experiment.

The rating methods, background light level, and stimulus temporal properties were the same as in our main experiment, and the three authors again served as observers. Each combination of modulation direction and frequency was presented five times, with trial order randomized. On 14 out of 154 trials, no modulation at all was shown (blank trials).

We replicated the visibility of the Purkinje tree for selective penumbral L and M cone stimulation (Figs 3 and 6), finding a maximum visibility rating at 16 Hz, dropping sharply at frequencies lower than 8 Hz and higher than 32 Hz. As in the main experiment, our open-field and penumbral L and M cone modulation elicits some spatial structure at frequencies higher than 16 Hz, but no Purkinje tree. Crucially, the *Melanopsin A* modulation elicited Purkinje-tree percepts similar to those produced by the penumbral L and M cone modulation. When penumbral cones were silenced but melanopsin driven at the same contrast (*Melanopsin B*), the Purkinje-tree percept was considerably reduced, with some observer variability in the degree of reduction. We speculate that the individual variability results from individual differences in the residual penumbral cone contrast produced by the *Melanopsin B* modulation. Out of the 14 blank trials, observers MS and GKA rated all of them as 0; observer DHB rated one trial out of the blank trials as 1, and 13 as 0.

Acknowledgments

We wish to thank Jessica Morgan and Grace Han for acquiring the fundus photographs of our naïve observer.

Author Contributions

Conceived and designed the experiments: MS GKA DHB. Performed the experiments: MS GKA DHB. Analyzed the data: MS GKA DHB. Wrote the paper: MS GKA DHB.

References

1. Snodderly DM, Weinhaus RS, Choi JC (1992) Neural-vascular relationships in central retina of macaque monkeys (Macaca fascicularis). J Neurosci 12: 1169–1193. PMID: 1556592

2. Bird AC, Weale RA (1974) On the retinal vasculature of the human fovea. Exp Eye Res 19: 409–417. doi: 10.1016/0014-4835(74)90050-5 PMID: 4426347

3. Ashton N (1957) Retinal vascularization in health and disease: Proctor Award Lecture of the Association for Research in Ophthalmology. Am J Ophthalmol 44: 7–17. doi: 10.1016/0002-9394(57)90426-9 PMID: 13469948

4. Adams DL, Horton JC (2003) The representation of retinal blood vessels in primate striate cortex. J Neurosci 23: 5984–5997. PMID: 12853416

5. Cornsweet TN (1970) Visual Perception. New York: Academic Press.

6. Purkinje J (1825) Beobachtungen und Versuche zur Physiologie der Sinne: Neue Beiträge zur Kenntnis des Sehens in subjectiver Hinsicht. Berlin: G. Reimer.

7. Purkinje J (1819) Beobachtungen und Versuche zur Physiologie der Sinne: Beiträge zur Kenntnis des Sehens in subjectiver Hinsicht. Prague: Johann Gottfried Calve.

8. Wade NJ, Brožek J (2001) Purkinje's vision: The dawning of neuroscience. Mahwah, NJ: Lawrence Erlbaum Associates.

9. Müller H (1854) Ueber einige Verhältnisse der Netzhaut bei Menschen und Thieren. Verhandlungen der Physikalisch-Medizinischen Gesellschaft zu Würzburg 4: 96–100.

10. Müller H (1855) Ueber die entoptische Wahrnehmung der Netzhautgefässe, insbesondere als Beweismittel für die Lichtperception für die nach hinten gelegenen Netzhautelemente. Verhandlungen der Physikalisch-Medizinischen Gesellschaft zu Würzburg 5: 411–447.

11. Walker CB (1940) Use of the Purkinje figures as test for separated retina and other intraocular pathology. American Journal of Ophthalmology 23: 803–804. doi: 10.1016/S0002-9394(40)92383-2

12. Talbot EM, Murdoch JR, Keating D (1992) The Purkinje vascular entoptic test: a halogen light gives better results. Eye 6: 322–325. doi: 10.1038/eye.1992.64 PMID: 1446770

13. Suzuki R (1941) Die klinische Bedeutung der Purkinjeschen Aderfigur. I. Die grundlegende Forschung über das entoptische Gesichtsfeld. Nippon Ganka Gakkai Zasshi [Acta Societatis Ophthalmologicae Japonicae] 45: 590–621.

14. Scheerer R (1924) Die entoptische Sichtbarkeit der Blutbewegung im Auge und ihre klinische Bedeutung. Klinische Monatsblätter für Augenheilkunde 73: 67–107.

15. Pagenstecher AH (1903) Ueber Staroperationen mit besonderer Berücksichtigung der Nachstaroperation. Zeitschrift für Augenheilkunde 10: 206–219.

16. Murillo-Lopez F, Maumenee AE, Guyton DL (2000) Perception of Purkinje vessel shadows and foveal granular pattern as a measure of potential visual acuity. J Cataract Refract Surg 26: 260–265. doi: 10.1016/S0886-3350(99)00341-7 PMID: 10683795

17. Kraupa E (1949) Ueber die Purkinje'schen Aderfiguren und die Doppelbeleuchtung in Ophthalmoskopie und Spaltlampenuntersuchung. Ophthalmologica 118: 318–320. doi: 10.1159/000300734 PMID: 15409054

18. Goldmann H (1972) Examination of the fundus of the cataractous eye. Am J Ophthalmol 73: 309–320. doi: 10.1016/0002-9394(72)90058-X PMID: 5013245

19. Ehrich W (1961) Netzhautgefäszschattenfigur und Makulachagrin als entoptische Funktionsprüfung. Documenta Ophthalmologica 15: 371–425. doi: 10.1007/bf00234354 PMID: 13889521

20. Ehrich W (1961) Entoptische Phänomene von klinischer Bedeutung. Med Klin 54: 31–32.

21. Ehrich W (1958) Methodische Richtlinien zur entoptischen Funktionsprüfung. Klinische Monatsblätter für Augenheilkunde 133: 396–401.

22. Comberg D, Ehrich W (1971) Welche Gesichtsfeldbereiche kann man mit der Netzhautgefässschattenfigur erfassen? Ophthalmologica 162: 140–145. doi: 10.1159/000306255 PMID: 5089746

23. Applegate RA, Bradley A, van Heuven WA, Lee BL, Garcia CA (1997) Entoptic evaluation of diabetic retinopathy. Invest Ophthalmol Vis Sci 38: 783–791. PMID: 9112972

24. Bowen SF (1963) Retinal entoptic phenomena. Archives of Ophthalmology 69: 551. doi: 10.1001/archopht.1963.00960040557003 PMID: 14014601

25. Atchison DA, Applegate RA (1997) Two new tests assist in the diagnosis of a small calibre vein occlusion. Clinical and Experimental Optometry 80: 49–52. doi: 10.1111/j.1444-0938.1997.tb04850.x

26.   Hilmantel G, Applegate RA, van Heuven WA, Stowers SP, Bradley A, et al. (1999) Entoptic foveal avascular zone measurement and diabetic retinopathy. Optom Vis Sci 76: 826–831. PMID: 10612403

27.   Applegate RA, Bradley A, van Heuven WA (1990) Entoptic visualization of the retinal vasculature near fixation. Invest Ophthalmol Vis Sci 31: 2088–2098. PMID: 2211006

28.   Kluxen G, Wilden E (1987) An entoptic test in diabetic patients. Diabetes Care 10: 800–801. PMID: 3428061

29.   Eber SI (1922) Autoophthalmoscopy—subjective examination of the retina. American Journal of Ophthalmology 5: 973–974. doi: 10.1016/s0002-9394(22)90950-x

30.   Drews LC (1941) Autofundoscopy. American Journal of Ophthalmology 24: 1403–1417. doi: 10.1016/s0002-9394(14)77452-5

31.   Drews LC (1943) Further observations on autofundoscopy (auto-ophthalmoscopy of Eber; Purkinje figure of Walker). American Journal of Ophthalmology 26: 1143–1154. doi: 10.1016/s0002-9394(43)90490-8

32.   Friedman B (1931) A test for retinal function in cataractous patients. Archives of Ophthalmology 5: 636–637. doi: 10.1001/archopht.1931.00820040132010

33.   Brodie SE (1987) Evaluation of cataractous eyes with opaque media. Int Ophthalmol Clin 27: 153–162. doi: 10.1097/00004397-198702730-00004 PMID: 3308746

34.   Goebel K (1922) Die Funktionsprüfung der zentralen Netzhautpartien auf entoptischem Wege. Archiv für Augenheilkunde 90: 245–249.

35.   Estévez O, Spekreijse H (1982) The "silent substitution" method in visual research. Vision Res 22: 681–691. doi: 10.1016/0042-6989(82)90104-3 PMID: 7112962

36.   Watson AB, Yellott JI (2012) A unified formula for light-adapted pupil size. Journal of Vision 12: 12. doi: 10.1167/12.10.12

37.   Kolb H (1995) Facts and Figures Concerning the Human Retina. In: Kolb H, Fernandez E, Nelson R, editors. Webvision: The Organization of the Retina and Visual System. Salt Lake City (UT).

38.   Kelly DH (1964) Sine waves and flicker fusion. Documenta Ophthalmologica 18: 16–35. doi: 10.1007/bf00160561 PMID: 14217806

39.   Kelly DH (1979) Motion and vision. II. Stabilized spatio-temporal threshold surface. Journal of the Optical Society of America 69: 1340–1349. doi: 10.1364/JOSA.69.001340 PMID: 521853

40.   Allefeld C, Putz P, Kastner K, Wackermann J (2011) Flicker-light induced visual phenomena: frequency dependence and specificity of whole percepts and percept features. Conscious Cogn 20: 1344–1362. doi: 10.1016/j.concog.2010.10.026 PMID: 21123084

41.   Brown CR, Gebhard JW (1948) Visual field articulation in the absence of spatial stimulus gradients. J Exp Psychol 38: 188–200. doi: 10.1037/h0054433 PMID: 18913668

42.   Young RS, Cole RE, Gamble M, Rayner MD (1975) Subjective patterns elicited by light flicker. Vision Res 15: 1291–1293. doi: 10.1016/0042-6989(75)90177-7 PMID: 1198944

43.   Smythies JR (1957) A preliminary analysis of the stroboscopic patterns. Nature 179: 523–524. doi: 10.1038/179523a0

44.   Remole A (1971) Luminance thresholds for subjective patterns in a flickering field: effect of wavelength. Journal of the Optical Society of America 61: 1164. doi: 10.1364/josa.61.001164 PMID: 5121886

45.   von Helmholtz H (1867) Handbuch der Physiologischen Optik. Leipzig: Leopold Voss.

46.   Coppola D, Purves D (1996) The extraordinarily rapid disappearance of entoptic images. Proc Natl Acad Sci U S A 93: 8001–8004. doi: 10.1073/pnas.93.15.8001 PMID: 8755592

47.   Steinbuch W (1813) Beiträge zur Physiologie des Auges: 1. Das Sehen des im eigenen Auge fliessendes Blutes. Jahrbücher der teutschen Medicin und Chirurgie 3: 270–285.

48.   Rood ON (1860) On a probable means of rendering visible the circulation in the eye. American Journal of Science and Arts 30: 264–265.

49.   Vierodt K (1856) Die Wahrnehmung des Blutlaufes in der Netzhaut des eigenen Auges. Archiv für physiologische Heilkunde 15: 255–268.

50.   Gudden B (1849) Ueber das Verhältniss der Centralgefäße des Auges zum Gesichtsfelde. Archiv für Anatomie, Physiologie und wissenschaftliche Medicin: 522–532.

51.   Exner S (1884) Die mangelhafte Erregbarkeit der Netzhaut für Licht von abnormer Einfallsrichtung. Sitzungsberichte der Kaiserlichen Akademie der Wissenschaften: Mathematisch-Naturwissenschaftliche Classe 88: 103–108.

52.   Deeley RM (1913) Retinal shadows? Nature 90: 594–594. doi: 10.1038/090594e0

53. Aubert H (1865) Physiologie der Netzhaut. Breslau: Morgenstern.

54. von Zehender W (1895) Ueber einige subjective Gesichtswahrnehmungen. II. Die Schattenbilder der Netzhautgefässe und der Eintrittsstelle des Sehnerven. Klinische Monatsblätter für Augenheilkunde 33: 112–125.

55. von Thomsen E (1919) Über Johannes Evangelista Purkinje und seine Werke. Skandinavisches Archiv für Physiologie 37: 1–116. doi: 10.1111/j.1748-1716.1919.tb00120.x

56. Kahn RH (1908) Beiträge zur Physiologie des Gesichtssinnes. I. Farbige Schatten auf der Netzhaut. Lotos 56: 1–10.

57. Exner S (1868) Ueber einige neue subjective Gesichtserscheinungen. Archiv für die Gesammte Physiologie des Menschen und der Thiere 1: 375–394. doi: 10.1007/bf01640325

58. Stigler R (1905) Eine neue subjektive Gesichtserscheinung. Zeitschrift für Psychologie und Physiologie der Sinnesorgane 39: 332–340.

59. Sharpe CR (1972) The visibility and fading of thin lines visualized by their controlled movement across the retina. J Physiol 222: 113–134. PMID: 5037063

60. Drysdale AE (1975) The visibility of retinal blood vessels. Vision Res 15: 813–818. doi: 10.1016/0042-6989(75)90259-X PMID: 1154661

61. Ditchburn RW (1936) Shadows of the retinal blood-vessels seen by monochromatic light. Nature 137: 661–661. doi: 10.1038/137661a0

62. Bradley A, Zhang H, Applegate RA, Thibos LN, Elsner AE (1998) Entoptic image quality of the retinal vasculature. Vision Res 38: 2685–2696. doi: 10.1016/S0042-6989(97)00345-3 PMID: 12116711

63. Wyatt HJ (1978) Purkinje's methods for visualizing the internal retinal circulation: A look at the source. Vision Research 18: 875–877. doi: 10.1016/0042-6989(78)90133-5 PMID: 676098

64. Cornsweet TN (1966) Stabilized image techniques. In: Whitcomb MA, editor. Recent Developments in Vision Research. Washington, DC: National Academy of Sciences.

65. Stockman A, Sharpe LT (2000) Spectral sensitivities of the middle- and long-wavelength sensitive cones derived from measurements in observers of known genotype. Vision Research 40: 1711–1737. doi: 10.1016/S0042-6989(00)00021-3 PMID: 10814758

66. CIE (2006) Technical Report 170–1: Fundamental chromaticity diagram with physiological axes—Part 1. Vienna: Central Bureau of the Commission Internationale de l' Éclairage.

67. Brainard DH, Stockman A (2010) Colorimetry. In: Bass M, DeCusatis C, Enoch J, Lakshminarayanan V, Li G et al., editors. The Optical Society of America Handbook of Optics, 3rd edition, Volume III: Vision and Vision Optics. New York: McGraw Hill. pp. 10.11–10.56.

68. Adams DL, Horton JC (2002) Shadows cast by retinal blood vessels mapped in primary visual cortex. Science 298: 572–576. doi: 10.1126/science.1074887 PMID: 12386328

69. Adams DL, Horton JC (2003) A precise retinotopic map of primate striate cortex generated from the representation of angioscotomas. J Neurosci 23: 3771–3789. PMID: 12736348

70. Gooley JJ, Ho Mien I, St Hilaire MA, Yeo SC, Chua EC, et al. (2012) Melanopsin and rod-cone photoreceptors play different roles in mediating pupillary light responses during exposure to continuous light in humans. J Neurosci 32: 14242–14253. doi: 10.1523/JNEUROSCI.1321-12.2012 PMID: 23055493

71. McDougal DH, Gamlin PD (2010) The influence of intrinsically-photosensitive retinal ganglion cells on the spectral sensitivity and response dynamics of the human pupillary light reflex. Vision Res 50: 72–87. doi: 10.1016/j.visres.2009.10.012 PMID: 19850061

72. Kankipati L, Girkin CA, Gamlin PD (2010) Post-illumination pupil response in subjects without ocular disease. Invest Ophthalmol Vis Sci 51: 2764–2769. doi: 10.1167/iovs.09-4717 PMID: 20007832

73. Kardon R, Anderson SC, Damarjian TG, Grace EM, Stone E, et al. (2009) Chromatic pupil responses: preferential activation of the melanopsin-mediated versus outer photoreceptor-mediated pupil light reflex. Ophthalmology 116: 1564–1573. doi: 10.1016/j.ophtha.2009.02.007 PMID: 19501408

74. Gamlin PD, McDougal DH, Pokorny J, Smith VC, Yau KW, et al. (2007) Human and macaque pupil responses driven by melanopsin-containing retinal ganglion cells. Vision Res 47: 946–954. doi: 10.1016/j.visres.2006.12.015 PMID: 17320141

75. Lucas RJ, Hattar S, Takao M, Berson DM, Foster RG, et al. (2003) Diminished pupillary light reflex at high irradiances in melanopsin-knockout mice. Science 299: 245–247. doi: 10.1126/science.1077293 PMID: 12522249

76. Hattar S, Lucas RJ, Mrosovsky N, Thompson S, Douglas RH, et al. (2003) Melanopsin and rod-cone photoreceptive systems account for all major accessory visual functions in mice. Nature 424: 76–81. doi: 10.1038/nature01761 PMID: 12808468

77.   Panda S, Sato TK, Castrucci AM, Rollag MD, DeGrip WJ, et al. (2002) Melanopsin (Opn4) require-
       ment for normal light-induced circadian phase shifting. Science 298: 2213–2216. doi: 10.1126/
       science.1076848 PMID: 12481141

78.   Hattar S, Liao HW, Takao M, Berson DM, Yau KW (2002) Melanopsin-containing retinal ganglion
       cells: architecture, projections, and intrinsic photosensitivity. Science 295: 1065–1070. doi: 10.1126/
       science.1069609 PMID: 11834834

79.   Berson DM, Dunn FA, Takao M (2002) Phototransduction by retinal ganglion cells that set the circadi-
       an clock. Science 295: 1070–1073. doi: 10.1126/science.1067262 PMID: 11834835

80.   Brown TM, Gias C, Hatori M, Keding SR, Semo M, et al. (2010) Melanopsin contributions to irradiance
       coding in the thalamo-cortical visual system. PLoS Biol 8: e1000558. doi: 10.1371/journal.pbio.
       1000558 PMID: 21151887

81.   Brown TM, Tsujimura S, Allen AE, Wynne J, Bedford R, et al. (2012) Melanopsin-based brightness
       discrimination in mice and humans. Curr Biol 22: 1134–1141. doi: 10.1016/j.cub.2012.04.039 PMID:
       22633808

82.   Horiguchi H, Winawer J, Dougherty RF, Wandell BA (2013) Human trichromacy revisited. Proc Natl
       Acad Sci U S A 110: E260–269. doi: 10.1073/pnas.1214240110 PMID: 23256158

83.   Allen AE, Storchi R, Martial FP, Petersen RS, Montemurro MA, et al. (2014) Melanopsin-driven light
       adaptation in mouse vision. Curr Biol 24: 2481–2490. doi: 10.1016/j.cub.2014.09.015 PMID:
       25308073

84.   Tsujimura S, Ukai K, Ohama D, Nuruki A, Yunokuchi K (2010) Contribution of human melanopsin reti-
       nal ganglion cells to steady-state pupil responses. Proc Biol Sci 277: 2485–2492. doi: 10.1098/rspb.
       2010.0330 PMID: 20375057

85.   Feigl B, Zele AJ (2014) Melanopsin-expressing intrinsically photosensitive retinal ganglion cells in reti-
       nal disease. Optom Vis Sci 91: 894–903. doi: 10.1097/OPX.0000000000000284 PMID: 24879087

86.   Feigl B, Zele AJ, Fader SM, Howes AN, Hughes CE, et al. (2012) The post-illumination pupil response
       of melanopsin-expressing intrinsically photosensitive retinal ganglion cells in diabetes. Acta Ophthal-
       mol 90: e230–234. doi: 10.1111/j.1755-3768.2011.02226.x PMID: 21883986

87.   Roecklein K, Wong P, Ernecoff N, Miller M, Donofry S, et al. (2013) The post illumination pupil re-
       sponse is reduced in seasonal affective disorder. Psychiatry Res 210: 150–158. doi: 10.1016/j.
       psychres.2013.05.023 PMID: 23809464

88.   Noseda R, Burstein R (2011) Advances in understanding the mechanisms of migraine-type photopho-
       bia. Curr Opin Neurol 24: 197–202. doi: 10.1097/WCO.0b013e3283466c8e PMID: 21467933

89.   Ecker JL, Dumitrescu ON, Wong KY, Alam NM, Chen S-K, et al. (2010) Melanopsin-expressing retinal
       ganglion-cell photoreceptors: cellular diversity and role in pattern vision. Neuron 67: 49–60. doi: 10.
       1016/j.neuron.2010.05.023 PMID: 20624591

90.   Barrionuevo PA, Nicandro N, McAnany JJ, Zele AJ, Gamlin P, et al. (2014) Assessing rod, cone, and
       melanopsin contributions to human pupil flicker responses. Invest Ophthalmol Vis Sci 55: 719–727.
       doi: 10.1167/iovs.13-13252 PMID: 24408974

91.   Provencio I, Rodriguez IR, Jiang G, Hayes WP, Moreira EF, et al. (2000) A novel human opsin in the
       inner retina. J Neurosci 20: 600–605. PMID: 10632589

92.   Provencio I, Rollag MD, Castrucci AM (2002) Photoreceptive net in the mammalian retina. Nature
       415: 493. doi: 10.1038/415493a PMID: 11823848

93.   Panda S, Nayak SK, Campo B, Walker JR, Hogenesch JB, et al. (2005) Illumination of the melanopsin
       signaling pathway. Science 307: 600–604. doi: 10.1126/science.1105121 PMID: 15681390

94.   Spitschan M, Jain S, Brainard DH, Aguirre GK (2014) Opponent melanopsin and S-cone signals in
       the human pupillary light response. Proc Natl Acad Sci U S A 111: 15568–15572. doi: 10.1073/pnas.
       1400942111 PMID: 25313040

95.   Tsujimura S, Tokuda Y (2011) Delayed response of human melanopsin retinal ganglion cells on the
       pupillary light reflex. Ophthalmic Physiol Opt 31: 469–479. doi: 10.1111/j.1475-1313.2011.00846.x
       PMID: 21645019

96.   Viénot F, Bailacq S, Rohellec JL (2010) The effect of controlled photopigment excitations on pupil ap-
       erture. Ophthalmic Physiol Opt 30: 484–491. doi: 10.1111/j.1475-1313.2010.00754.x PMID:
       20883331

97.   Smithson HE (2014) S-cone psychophysics. Vis Neurosci 31: 211–225. doi: 10.1017/
       S0952523814000030 PMID: 24759446

98.   Martin PR, Lee BB (2014) Distribution and specificity of S-cone ("blue cone") signals in subcortical vi-
       sual pathways. Vis Neurosci 31: 177–187. doi: 10.1017/S0952523813000631 PMID: 24555883

99.   Ishihara S (1977) Tests for Colour-Blindness. Tokyo: Kanehara Shuppen Company, Ltd.

100. Donner KO, Rushton WA (1959) Retinal stimulation by light substitution. J Physiol 149: 288–302. PMID: 13817555

101. ISO (2007) Ophthalmic instruments—Fundamental requirements and test methods. Part 2: Light hazard protection (ISO 15004–2). Geneva: International Organization for Standardization.

102. Viénot F, Brettel H, Dang TV, Le Rohellec J (2012) Domain of metamers exciting intrinsically photosensitive retinal ganglion cells (ipRGCs) and rods. J Opt Soc Am A Opt Image Sci Vis 29: A366–376. doi: 10.1364/JOSAA.29.00A366 PMID: 22330402

103. Viénot F, Brettel H (2014) The Verriest Lecture: Visual properties of metameric blacks beyond cone vision. J Opt Soc Am A Opt Image Sci Vis 31: A38–46. doi: 10.1364/JOSAA.31.000A38 PMID: 24695197

104. Brainard DH (1997) The Psychophysics Toolbox. Spat Vis 10: 433–436. doi: 10.1163/156856897X00357 PMID: 9176952

105. Rushton WA, Henry GH (1968) Bleaching and regeneration of cone pigments in man. Vision Res 8: 617–631. doi: 10.1016/0042-6989(68)90040-0 PMID: 5729910

106. Kaiser PK, Boynton RM (1996) Human Color Vision. Washington, D.C.: Optical Society of America.

107. Prahl S (1999) Optical absorption of hemoglobin. Oregon Medical Laser Center.

108. Hill AV (1910) The possible effects of the aggregation of the molecules of hæmoglobin on its dissociation curves. J Physiol 40: iv–vii.

109. Lucas RJ, Peirson SN, Berson DM, Brown TM, Cooper HM, et al. (2014) Measuring and using light in the melanopsin age. Trends Neurosci 37: 1–9. doi: 10.1016/j.tins.2013.10.004 PMID: 24287308

110. Govardovskii VI, Fyhrquist N, Reuter T, Kuzmin DG, Donner K (2000) In search of the visual pigment template. Visual Neuroscience 17: 509–528. doi: 10.1017/s0952523800174036 PMID: 11016572

111. Enezi J, Revell V, Brown T, Wynne J, Schlangen L, et al. (2011) A "melanopic" spectral efficiency function predicts the sensitivity of melanopsin photoreceptors to polychromatic lights. J Biol Rhythms 26: 314–323. doi: 10.1177/0748730411409719 PMID: 21775290

112. Bailes HJ, Lucas RJ (2013) Human melanopsin forms a pigment maximally sensitive to blue light ($\lambda_{max} \approx 479$ nm) supporting activation of $G_{q/11}$ and $G_{i/o}$ signalling cascades. Proc Biol Sci 280: 20122987. doi: 10.1098/rspb.2012.2987 PMID: 23554393

113. Brown TM, Allen AE, al-Enezi J, Wynne J, Schlangen L, et al. (2013) The melanopic sensitivity function accounts for melanopsin-driven responses in mice under diverse lighting conditions. PLoS One 8: e53583. doi: 10.1371/journal.pone.0053583 PMID: 23301090

114. Do MT, Kang SH, Xue T, Zhong H, Liao HW, et al. (2009) Photon capture and signalling by melanopsin retinal ganglion cells. Nature 457: 281–287. doi: 10.1038/nature07682 PMID: 19118382

115. Webster MA, MacLeod DI (1988) Factors underlying individual differences in the color matches of normal observers. J Opt Soc Am A 5: 1722–1735. doi: 10.1364/JOSAA.5.001722 PMID: 3204435

116. Xu J, Pokorny J, Smith VC (1997) Optical density of the human lens. J Opt Soc Am A Opt Image Sci Vis 14: 953–960. doi: 10.1364/JOSAA.14.000953 PMID: 9114506